International Journal of Plasticity 120 (2019) 205–219

Contents lists available at ScienceDirect

International Journal of Plasticity

journal homepage: www.elsevier.com/locate/ijplas

Application of artificial neural networks in micromechanics for polycrystalline metals

Usman Ali, Waqas Muhammad, Abhijit Brahme, Oxana Skiba, Kaan Inal*

University of Waterloo, 200 University Ave W, Waterloo, On, N2L 3G1, Canada

ARTICLE INFO

Keywords:
Artificial neural network
Crystal plasticity
Texture
Aluminium alloys

ABSTRACT

Machine learning techniques are widely used to understand and predict data trends and therefore can provide a huge computational advantage over conventional numerical techniques. In this work, an artificial neural network (ANN) model is coupled with a rate-dependant crystal plasticity finite element method (CPFEM) formulation to predict the stress-strain behavior and texture evolution in AA6063-T6 under uniaxial tension and simple shear. Firstly, stress-strain and texture evolution results from the crystal plasticity simulations were verified with experimental observations for AA6063-T6 under simple shear and tension. Next, results from crystal plasticity simulations were used to train, validate and test the ANN model. The proposed ANN framework, was successfully applied on single crystal simulation results to predict stress-strain and texture data. Then, the proposed ANN framework was applied to predict the stress-strain curves and texture evolution of AA6063-T6 during uniaxial tension and simple shear. The flexibility of the proposed ANN model was also tested, for simple shear, with a completely new data set and the predicted results showed excellent agreement with corresponding crystal plasticity simulations. Finally, the predictive capability of the proposed model was further demonstrated by successfully validating the ANN model for non-proportional loading paths such as uniaxial tension followed by simple shear and simple shear followed by tension. The results presented in this research clearly demonstrate that the proposed ANN model provided significant computational time improvements without any major sacrifice in accuracy.

1. Introduction

Interest in Machine learning (ML) models to understand and predict the material behavior and properties has grown rapidly in recent years. Artificial neural network (ANN) is one group of algorithms used for Machine learning (ML). ANN frameworks model the data using mathematical models that try to simulate a neuron in the brain. In the brain, the process of knowledge acquiring, or learning, for a particular task occurs through experience and does so till we reach the required objective. Such approaches attempt to establish relations from simulated or experimental data using computing systems with learning capabilities. Similar to conventional simulation tools such as FE etc, computing systems such as ANN provide an alternative way to accurately assess the material properties as well as to design new materials in an accelerated manner. Some applications of ANN modelling in the context of material science have been evaluated by Bhadeshia (1999) and Raabe (2002). Specifically, ANN models could be used with complex problems with nonlinear correlations and interactions between inputs and outputs. For example, Lin et al., 2008a, 2008b use ANN to predict material flow behavior for low alloy steel at elevated temperature and show good agreement between experimental and ANN

* Corresponding author.
E-mail address: kinal@uwaterloo.ca (K. Inal).

https://doi.org/10.1016/j.ijplas.2019.05.001
Received 5 November 2018; Received in revised form 4 May 2019; Accepted 5 May 2019
Available online 08 May 2019

results. Similarly, Haghdadi et al. (Haghdadi et al., 2013) use ANN to predict the flow behavior of cast A356 aluminum alloy under various thermomechanical conditions while Jenab et al. (2013) use ANN to predict the hot deformation of AA7075 at low strain rates. High temperature flow behavior of AZ31 and ZK60 magnesium alloys were also predicted using various ANN approaches (Sabokpa et al., 2012; Qin et al., 2010).

It is well known that microstructure plays an important role in defining the material behavior under different strain-paths. A number of studies have been done to relate the flow behavior to the microstructure using ANN techniques. Reddy et al. (2005) used ANN to predict the grain size as a function of various alloying elements in Al–7Si and show decent predictions. Brahme et al. (2009) have used ANNs for the prediction of cold rolling textures of steels as a function of varying carbon content and carbide dispersion. Cetinel et al. (Çetinel et al., 2002) used ANN to predict the phases, strength and tempering temperature of AISI 1020 steel bars treated by the Tempcore process. Guessasma and Coddet (2004) successfully used an ANN model to predict various phases and process outputs during Atmospheric Plasma Spray (APS) of alumina–titania coatings. Liu et al. (2015) solved the inverse ANN problem to find optimum microstructure for desired material properties in Galfenol. Furthermore, Yassar et al. (2010) employed an ANN model to predict flow stress properties of AA6062 as a function of dislocation structure thus avoiding the computationally expensive dislocation plasticity models.

Various published works discussed above show the predictive capability of ANN models. However, to the best knowledge of authors, there are no works on the predictive capability of ANN models to capture the polycrystalline material behavior and microstructure evolution in real materials. In this work, artificial neural network based machine learning framework is used in conjunction with validated crystal plasticity data to predict the stress-strain behavior and texture evolution in AA 6063 – T6 under tension and shear. To obtain reliable data sets for the proposed ANN model, crystal plasticity based finite element simulations were performed and validated with experimental results. To check the effectiveness of the ANN model, single crystal stress-strain and texture data from crystal plasticity simulations were used to train, validate and test the ANN model and showed good agreements. Next, experimentally validated stress-strain and texture data from polycrystalline AA6063-T6 crystal plasticity simulations was used to train, validate and test the ANN model. ANN model showed excellent agreement with polycrystalline simulations under tension and shear and successfully captured the stress-strain and texture evolution. It should also be mentioned that the ANN model was also used to perform predictions outside the boundaries of the trained model; these predictions with the ANN model showed excellent agreement with simulated results. As a final application, the proposed ANN model was also used to successfully predict the material response under non-proportional loading paths such as uniaxial tension-simple shear and simple shear-uniaxial tension. The runtime comparison between ANN and crystal plasticity simulations showed computational savings up to 99.9%; this highlights the computational advantage of using ANN models over conventional numerical simulations.

This work provides a viable solution to speedup numerical simulations to save computational time and resources. Computational advantages from the proposed framework can be used to perform full scale component level simulations at a fraction of time cost compared to crystal plasticity simulations. The significance of this work lies in the fact that with the computational savings while still maintaining the accuracy of the prediction, the proposed framework can be used for alloy development and material design. Finally, the authors would like to mention that, while the accuracy of the crystal plasticity model employed in this study could be further improved, the main focus of this research is to incorporate ANN into crystal plasticity theory to significantly improve CPU time.

2. Methods for generating data sets

The applicability and quality of any Machine Learning prediction technique strongly depends on the precision and size of the data set. In most cases, the precision of the machine learning technique is directly proportional to the size and accuracy of the data set. Therefore, before designing an artificial neural network (ANN) based machine learning model, the sample data must be carefully collected. The network can only be as accurate as the data used to train, validate and test the network. Also, the data set should contain sufficient information that is representative and descriptive of the mechanical process. If the above conditions are true, then and only then the trained ANN model would be able to reproduce and predict new results (Ghaboussi et al., 1991).In this work, an in-house crystal plasticity framework is used to obtain a representative and accurate data set. Stress-strain and texture results from crystal plasticity simulations are compared to experimental results to validate the accuracy of the simulated results.

2.1. Experimental texture and stress-strain results

In this work, stress-strain and texture evolution data of commercially available extruded AA6063 – T6 (Fig. 1) material under uniaxial tension and simple shear were used. Starting (extruded) material shows high amounts of Cube and Goss texture components with equiaxed grain morphology (Fig. 1). Experimental methodology and procedure for obtaining the stress-strain and texture

Fig. 1. Electron backscatter diffraction (EBSD) inverse pole figure (IPF) map of the initial microstructure.

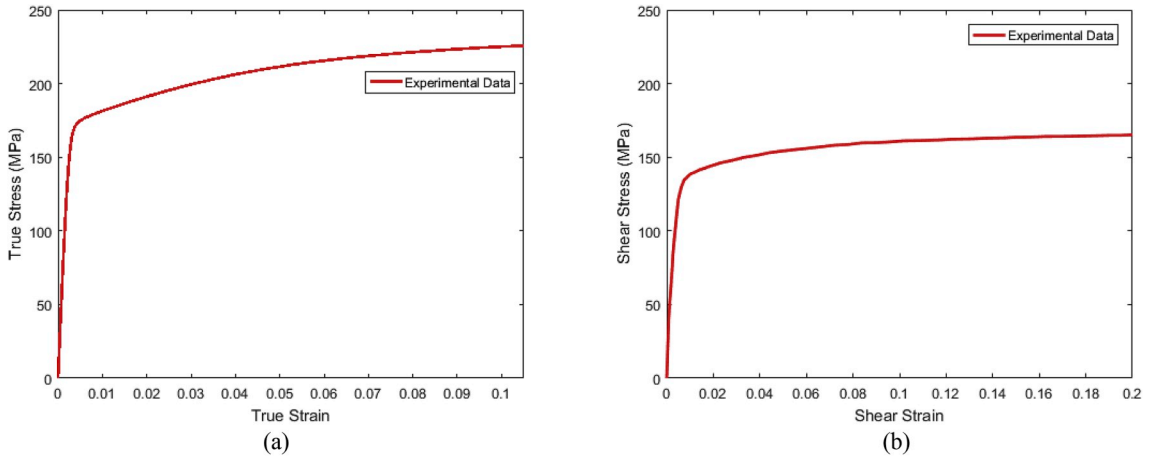

Fig. 2. Uniaxial stress-strain curves for AA6063 – T6 under (a) Uniaxial tension (b). Simple shear.

evolution data used in this work has been outlined in a previous work from this group by Muhammad et al. (2017). Fig. 2a and b show the uniaxial tensile and simple shear stress-strain curves respectively. Fig. 3a–c shows the initial and final < 1 1 1 > pole figures under uniaxial tension and simple shear. Fig. 3b shows the uniaxial tensile < 1 1 1 > pole figure at 10% strain. Pole figure results after tension do not show any major changes in the texture. However, there is a decrease in the overall intensity. Fig. 3c shows the < 1 1 1 > pole figure after 20% shear strain. As reported in a recent study (Muhammad et al., 2017), pole figure results at 20% shear strain show rotation of Cube and Goss components with respect to the normal direction.

2.2. Crystal plasticity constitutive model

Various numerical methods have been proposed to capture the flow behavior of materials. In this regard, phenomenological models are the most widely used and have successfully captured material behavior under various deformations (Ghaffari Tari et al., 2014; Plunkett et al., 2008). However, phenomenological models are unable to capture the texture evolution during deformation. Crystal plasticity formulations account for material plastic deformation using crystallographic slip and therefore can predict the stress-strain behavior and texture evolution. Several works (Ali et al., 2017; Akpama et al., 2016; Diard et al., 2005) in literature have shown the power of such models to predict material behavior under various deformation modes for FCC, BCC and HCP materials.

The rate-dependent crystal plasticity formulation used in this work is based on the formulation by Asaro and Needlemen (Asaro and Needleman, 1985). In this model, plastic deformation occurs due to 12 < 110 > and < 111 > slip systems where the elastic constitutive equation can be written as:

$$\hat{\boldsymbol{\sigma}} = \boldsymbol{LD} - \dot{\boldsymbol{\sigma}}^{0} - \boldsymbol{\sigma}\, tr\boldsymbol{D} \tag{1}$$

where $\hat{\boldsymbol{\sigma}}$ is the Jaumann rate of Cauchy stress, $\boldsymbol{D}$ is the strain-rate tensor, $\boldsymbol{L}$ is the elastic stress tensor and $\dot{\boldsymbol{\sigma}}^{0}$ is the viscoplastic type stress state.

Slip rates for each slip system α are calculated as:

$$\dot{\gamma}_{\alpha} = \dot{\gamma}_{0} sgn\ \tau_{\alpha} \left| \frac{\tau_{\alpha}}{g_{\alpha}} \right|^{1/m} \tag{2}$$

where $\dot{\gamma}_{0}$ is the reference shear rate, τ_{α} is the resolved shear stress on each slip system, m is the strain-rate sensitivity index and g_{α} is the hardness of each slip system.

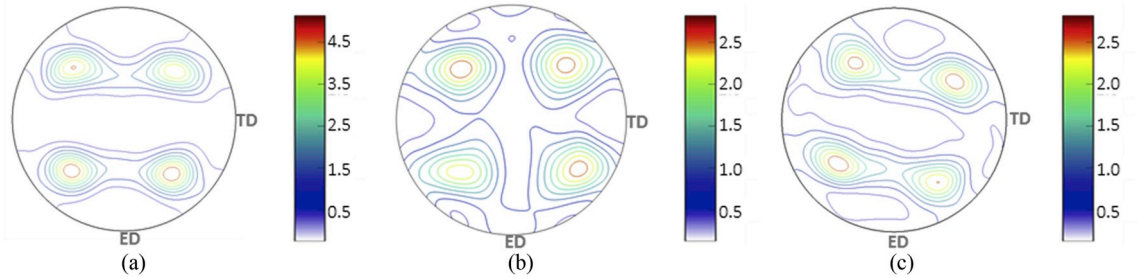

Fig. 3. (a) Initial < 1 1 1 > pole figure for AA6063-T6 (b). Final < 1 1 1 > pole figure for AA6063-T6 after tension (c). Final < 1 1 1 > pole figure for AA6063-T6 after 20% simple shear.

Similarly, work hardening is calculated as:

$$\dot{g}_\alpha = \sum_\beta h_{\alpha\beta}|\dot{\gamma}_\beta| \tag{3}$$

where $h_{\alpha\beta}$ are the hardening moduli such as:

$$h_{\alpha\beta} = q_{\alpha\beta}h_\beta \text{ (no sum on } \beta) \tag{4}$$

where $q_{\alpha\beta}$ defines the latent hardening behavior of the crystal and h_β is the single crystal hardening rate.

$$q_{\alpha\beta} = \begin{bmatrix} A & qA & qA & qA \\ qA & A & qA & qA \\ qA & qA & A & qA \\ qA & qA & qA & A \end{bmatrix}$$

where, A is the 3 × 3 unity matrix and q is the ratio of latent hardening to self-hardening and is set to 1.

Lastly, single slip hardening used in this work is based on (Chang and Asaro, 1981) and is defined as:

$$h_\beta = h_s + (h_0 - h_s)sech^2\left[\left(\frac{h_0 - h_s}{\tau_s - \tau_0}\right)\gamma_\alpha\right] \tag{5}$$

where h_0 and h_s are the initial and asymptotic hardening rates, τ_s is the saturation value of the shear stress, if $h_s = 0$, and γ_α is the accumulated slip on a slip system. A more detailed description of the crystal plasticity model can be found in (Inal et al., 2002; Rossiter et al., 2010).

The crystal plasticity constitutive model explained above is integrated into an in-house crystal plasticity based finite element model (CPFEM). Contrary to other crystal plasticity models that employ homogenization (i.e., Taylor type, visco-plastic self-consistent), CPFEM has the advantage of capturing the inhomogeneous local distribution of strain and stress in the polycrystal (especially within the grains). Thus, due to the nature of the model, it is expected that CPFEM can produce more accurate predictions of the large strain phenomena compared to other models based on homogenization approaches. The CPFEM model employed in this study is a two-dimensional plane stress model and the details of the numerical formulation are presented in the work by Inal et al. (2002).

3. Artificial neural network (ANN) model

A feed forward back propagation ANN, used in this study, is a general method of non-parametric regression method (Cherkassky and Lari-Najafi, 1990). Artificial neural networks are a machine learning approach used to approximate non-linear functions. ANN models try to simulate the flow of information inside the brain by defining a set of neurons (in layers) as functions that output data based on inputs. Fig. 4 shows a typical single layer neural network where the inputs in the input layer and outputs from the output layer are connected by one hidden/internal layer. These neurons are massively interconnected and improve their predictive capability as the network evolves (Specht, 1991).

The outputs in an ANN model are connected to the inputs by a function $\boldsymbol{f}$. In simple terms, in ANN, the function $\boldsymbol{f}$ maps an input vector $\boldsymbol{x} \in \mathbb{R}^d$ into the corresponding output vector $\boldsymbol{y} \in \mathbb{R}^d$. The function $\boldsymbol{f}$ is found by minimizing the cost function C. The cost function C relates the difference between the network output $\boldsymbol{f}$ $(\boldsymbol{x})$ and the target value $\boldsymbol{y}$. The overall cost function C is calculated as an average of the individual cost functions C_x for each training sample x over the entire dataset:

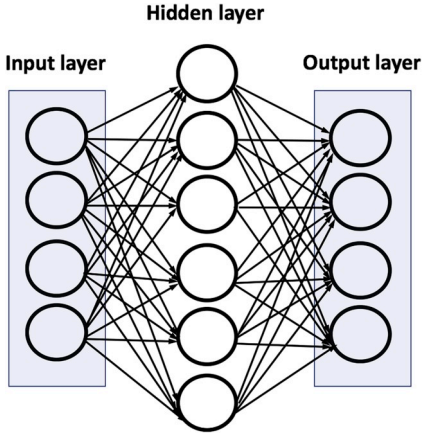

Fig. 4. Artificial neural network visualization for single layer.

$$C = \frac{1}{n}\sum_{x} C_x \tag{6}$$

In certain cases, the cost function can also contain a regularization term that prevents overfitting. This extra term usually acts as a penalty for the overall complexity of the model resulting in higher computational times for learning (Bishop, 2006).

The ANN function $\boldsymbol{f}$ is implemented by a directed set of interconnected units called artificial neurons (Bishop, 2006). The neurons are put in a layered architecture. Each neuron implements a basic computation and produces the output:

$$y = \varphi\left(\sum_{i=1}^{d} w_i x_i + b_i\right) \tag{7}$$

where w_i and b_i are the weights and bias of the i -th input in the ANN model, d is the number of elements in the input vector, x, and φ is a transfer, or an activation function. This output, from one layer, represents an input to the neurons of another layer, or an element of the output vector of the ANN. A sample ANN model with 1 layer and 4 inputs and outputs is shown in Fig. 4.

The relation between inputs and outputs in the layered architecture is implemented as:

$$\boldsymbol{a_j} = \boldsymbol{\phi}(\boldsymbol{w_j}\cdot\boldsymbol{a_{j-1}} + \boldsymbol{b_j}) \text{ for } 1 \le j \le L \text{ and } \mathrm{a}_0 = x \; 1 \le j \le L \; \mathrm{a}_0 = x \tag{8}$$

where L is the number of layers and $\boldsymbol{a}_L$ are the activation vectors for each neuron in layer L.

Accordingly, output in a layered structure can be written as:

$$\mathbf{y} = \varphi(\boldsymbol{V}\cdot\boldsymbol{a_L}) \tag{9}$$

where $\boldsymbol{V}$ are model parameters.

The weight matrices $\boldsymbol{w}_1, \ldots, \boldsymbol{w_L}$, the vectors of biases $\boldsymbol{b}_1, \ldots, \boldsymbol{b_L}$ and matrices $\boldsymbol{V}$ are learned from the input data set $\boldsymbol{x}$ for each layer in the ANN model. A neural network learns its weights and biases one sample at a time and tries to find the optimal function $\boldsymbol{f}$. In this work, backpropagation algorithm (a modification of gradient descent algorithm) is used for computing the cost function gradients that are used to converge to an optimal function. Backpropagation algorithms are used as they have been proven to be faster than other such algorithms (Rumelhart et al., 1988). In essence, backpropagation algorithms use the partial derivative of the cost function $\boldsymbol{C}$ for each layer with respect to any weight $\boldsymbol{w_L}$ $(\partial \boldsymbol{C}/\partial \boldsymbol{w})$ or bias $\boldsymbol{b_L}$ $(\partial \boldsymbol{C}/\partial \boldsymbol{b})$ in the network. This shows how fast the cost function changes when the weights and biases are changed (Rumelhart et al., 1988). By iteratively adjusting the weights and biases, the cost function $\boldsymbol{C}$ is minimized. Generally, an average squared error between the network outputs $\boldsymbol{f}$ $(\boldsymbol{x})$ and the target values $\boldsymbol{y}$ is chosen as the cost function. Although, the term for the partial derivative of the cost function could be complex, it gives detailed insights into the overall behavior of the artificial network (Nielsen, 2015).

Finally, the transfer function φ for each neuron, is chosen as a hyperbolic tangent sigmoid function:

$$\varphi(n) = \frac{2}{(1 + e^{-2n})} - 1 \tag{10}$$

This function is mathematically equivalent to hyperbolic tangent function and has stronger gradient, or higher derivative, than the standard logistic function, which allows faster optimization of the network (LeCun et al., 2012; Montavon and Müller, 2012).

ANN models are very sensitive to input data. Therefore, it is preferred practice to normalize or standardize the input dataset $\boldsymbol{x}$. The process of standardization is applied when the data follows normal distribution. Whereas normalization is required when there is big difference in the ranges of the input data. In this work, all the data was normalized in the range of $[-1 \; 1]$.

ANN models work by splitting the input data into training, validation and test sets. Training set is used to find the bias and weights to minimize the cost function C between the network's output f $(\boldsymbol{x})$ and the target value $\mathbf{y}$. The validation set is used to check the accuracy of the fitted parameters. In addition, validation set prevents the network from overfitting of data. The test set is used to measure the effectiveness of the model. Test set measures the predictive capability of the ANN model by using the generalization error (E_G) that evaluates the ability of the ANN model to predict outcome values for previously unseen data. This error usually has the form:

$$E_G = \frac{1}{n}\sum_{i=1}^{n} l(\mathbf{y}_i - f(\boldsymbol{x}_i)) \tag{11}$$

where l is the loss function used to calculate the error between the network's output f $(\boldsymbol{x})$ and the target value $\mathbf{y}$.

In this work, a mean-squared error function (MSE) (Hansen et al., 2013) is used to calculate E_G written as:

$$E_G = \frac{1}{n}\sum_{i=1}^{n} (\mathbf{y}_i - f(\boldsymbol{x}_i))^2 \tag{12}$$

Inputs to the ANN model used in this work comprises of the strain ε and the initial microstructure represented by a set of three Euler angles ϕ_1, ϕ, ϕ_2. Therefore, each data sample is presented by the vector $(\varepsilon, \phi_1, \phi, \phi_2)$. The number of such samples per strain point are determined by the number of elements in the representative microstructure. It is important to mention that as mentioned earlier, there should be sufficient data to completely capture the deformation process that is to be predicted. Similarly, the outputs $\boldsymbol{y}$ from the ANN model include the stresses σ and evolved microstructure of each crystal, i.e. $\boldsymbol{y} = (\sigma, \; \phi_1, \phi, \phi_2)$. A schematic representation of the proposed ANN framework with 1 hidden layer is shown in Fig. 5.

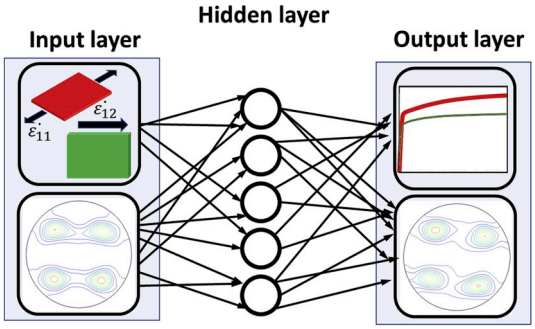

Figure 5. Schematic for the proposed ANN framework used in this work.

It should be noted that, there are several machine learning techniques available today (soft max, ReLU, etc.). While some techniques can be used with minor modifications, other techniques are not suitable for this specific type of data set. In this current work, artificial neural networks were used due to their flexibility to conform to *any* type of data set and their success with various mechanical problems. Furthermore, the performance of the machine learning model was validated for extrapolated predictions and the model employed in the research provided the most accurate predictions compared to other machine learning methods.

4. Results and discussion

4.1. Crystal plasticity model results

In this study, an EBSD map with 280 grains (Fig. 1) was used (Muhammad et al., 2017; Popova et al., 2015). The EBSD scan covering an area of 2800 by 500 μm was mapped onto 3500 quadrilateral elements (20 μm × 20 μm) where each element was assigned a set of Euler angles (ϕ_1, ϕ, ϕ_2) from the experimental EBSD data to incorporate the overall texture into the CPFEM. Next, $\dot{\varepsilon}_{11}$ and $\dot{\varepsilon}_{12}$ were applied to the CPFEM to simulate uniaxial tension and simple shear respectively. Corresponding crystal plasticity parameters used for the tensile and shear simulations are given in Table 1.

Texture and crystal plasticity simulation framework discussed in this section are used to validate the crystal plasticity simulation results with experimental results. Crystal plasticity simulation results are validated under uniaxial tension and simple shear and are presented in the following sections.

4.1.1. Uniaxial tension

Fig. 6 shows the experimental and simulated stress-strain response and texture evolution of AA6063-T6 under uniaxial tension. Fig. 6a shows the simulated and experimental stress-strain response. Simulated results show good agreement with experimental data. Fig. 6b and c show the experimental and simulated < 1 1 1 > pole figures respectively. Simulated and experimental pole figures show good agreement and capture the decrease in Goss texture component after uniaxial tension while, the overall intensity was predicted to be slightly lower than the experimental results. It is well known that, the accuracy of the predictions with CPFEM can be improved by using a larger EBSD maps (more grains) as input; however, this is not the main goal of this research.

4.1.2. Shear test

Fig. 7 shows the experimental and simulated stress-strain response and texture evolution of AA6063-T6 under simple shear. Fig. 7a shows the simulated and experimental stress-strain response. Simulated results show good agreement with experimental data with minor deviations near the yield point. Fig. 7 b & c show the experimental and simulated < 1 1 1 > pole figures respectively. Simulated and experimental pole figures show good agreement in pole figure trend and intensities and are able to predict the clockwise texture rotation about the normal direction accurately. The simulated results show similar rotation (11°) than experimental data (12°). In addition, simulated results capture the rotation in Cube texture and weakening of Goss texture component after shear (Rossiter et al., 2010).

The uniaxial tension and simple shear crystal plasticity stress-strain and texture results presented in this section show good agreement with experimental results for both strain-paths. Such agreement with experimental results provides the confidence to use the simulated data to train, validate and test the ANN model. In addition, validation of the ANN model with crystal plasticity results would automatically validate the ANN model to experimental data.

Table 1
Simulation parameters used in the crystal plasticity simulations for uniaxial tension and simple shear.

	m	q	h_0/τ_0	h_s/τ_0	τ_s/τ_0	τ_0
Value	0.02	1.0	2.08	0.14	1.18	61.0

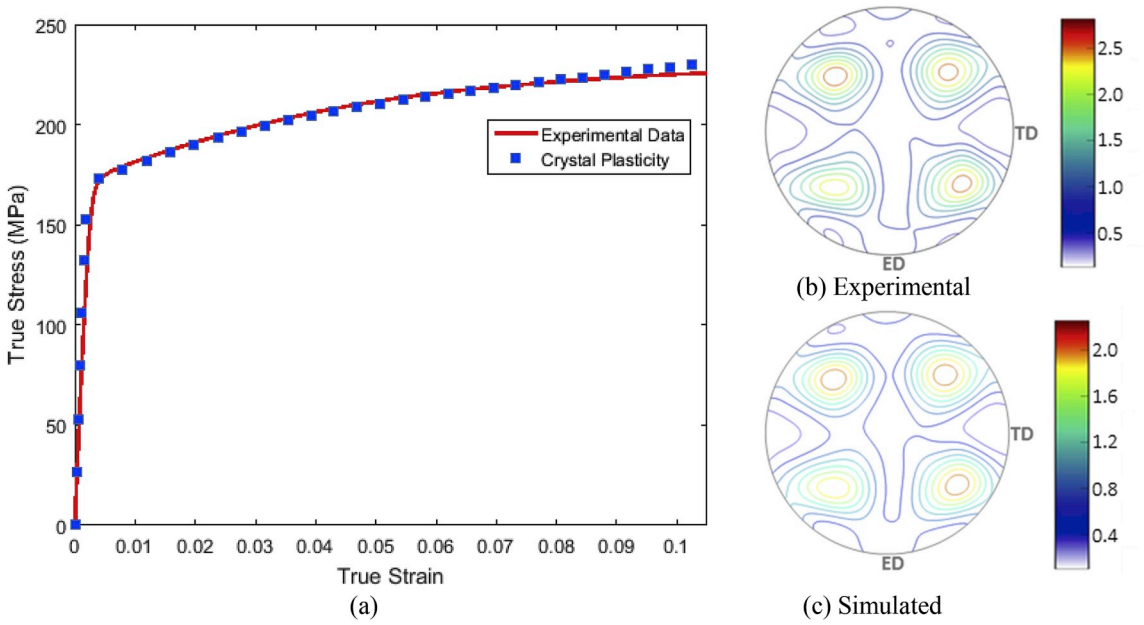

Fig. 6. (a) Experimental and simulated uniaxial tension stress-strain curves and (b) Experimental and (c) Simulated < 1 1 1 > pole figures under uniaxial tension.

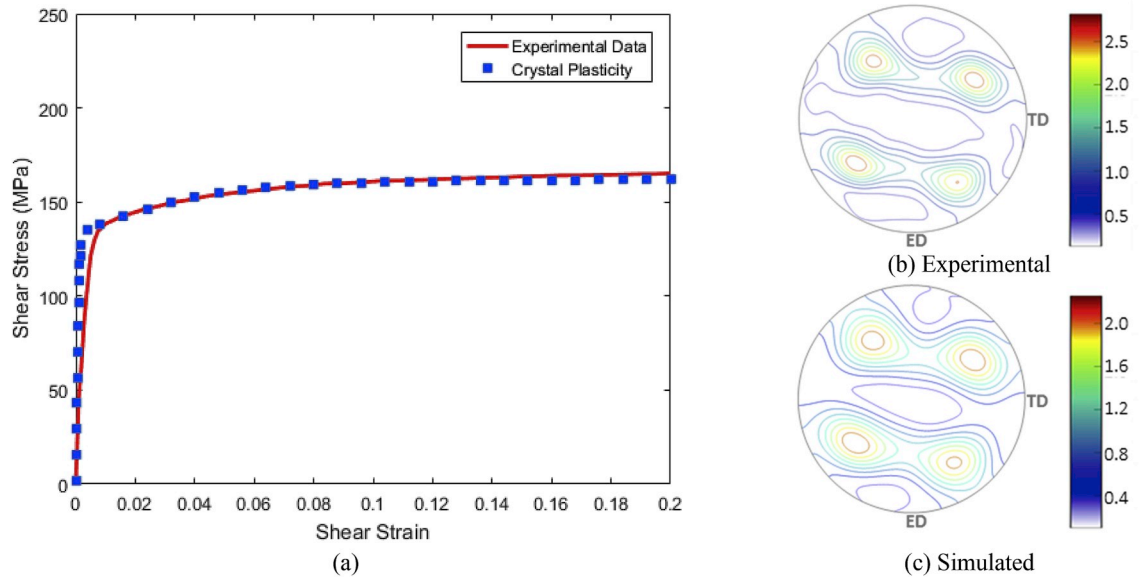

Fig. 7. (a) Experimental and simulated simple shear stress-strain curves and (b) Experimental and (c) Simulated < 1 1 1 > pole figures under simple shear.

4.2. Artificial neural network results

As mentioned in the previous sections, ANN models require an accurate and representative data sets to be trained on. In the aforementioned work, it has been shown that crystal plasticity simulations are able to accurately predict experimental stress-strain and texture results. Therefore, results from crystal plasticity simulations can be used to train, validate and test the ANN model to predict real material behavior. The proposed model was first tested on single crystal. The results are presented in Section 3.2.1. Next, the proposed model was applied to AA6063-T6 polycrystal under uniaxial tension and shear and the results are presented in Section 3.2.2.

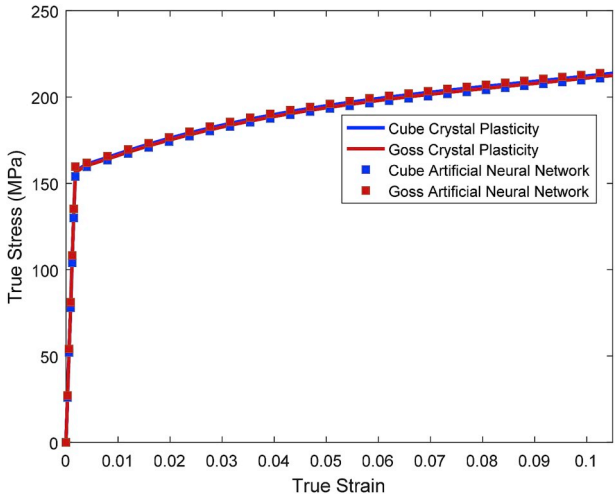

Fig. 8. Comparison between crystal plasticity and artificial neural network single crystal stress-strain curves under uniaxial tension.

4.2.1. ANN prediction for single crystal under tension and shear deformation

Single crystal responses were first used to verify the effectiveness of the ANN model under tension and shear. Crystal plasticity simulations for Cube (0°, 0°, 0°) and Goss (0°, 45°, 0°) orientations were simulated under tension and shear up to 10% and 20% strain respectively. Crystal plasticity data was parsed at random between the training (75%), validating (15%) and testing (15%) data sets for the ANN model using 80 neurons.

Fig. 8 shows the crystal plasticity and ANN stress-strain response for Cube and Goss under tension. Results in Fig. 8 demonstrate that ANN predictions show very good agreement with crystal plasticity results. Fig. 9 shows the crystal plasticity and ANN texture evolution predictions for Cube and Goss orientations using the < 1 1 1 > point pole figures. ANN predictions show good agreement with crystal plasticity results and are able to capture the complete trends. Mean square errors (MSE) between the ANN and crystal plasticity predictions were also calculated and are given in Table 2. MSE for uniaxial tension in Table 2 are on the order of 10^{-5} for the stress-strain predictions and 10^{-4} for texture predictions for both Cube and Goss thus confirming the accuracy of ANN predictions.

Literature shows that uniaxial tension does not exhibit a lot of texture evolution (Ali et al., 2017; Pandey et al., 2012). Therefore, for a better understanding of the strength of the ANN model, shear tests were simulated using the ANN model and are presented below. Simple shear provides an added level of complexity as simple shear results in a clockwise rotation in the overall texture in the < 1 1 1 > pole figure (Muhammad et al., 2017).

Fig. 10 shows the crystal plasticity and ANN stress-strain response for Cube and Goss under simple shear and shows that ANN predictions show very good agreement with crystal plasticity results. Fig. 11 shows the crystal plasticity and ANN texture evolution predictions for Cube and Goss orientations using < 1 1 1 > point pole figures at 10% and 20% strain. Two strain levels are chosen to show the increase in rotation of texture caused due to increased shear strain (Fig. 11). ANN texture predictions in Fig. 11 show good agreement with crystal plasticity results and are able to capture the texture rotation. It is noted that the MSE (Table 2) for ANN model under shear are higher than tension but still on the order of 10^{-5} for the stress-strain predictions and 10^{-4} for texture predictions for both Cube and Goss thus confirming the accuracy of ANN predictions for different strain paths.

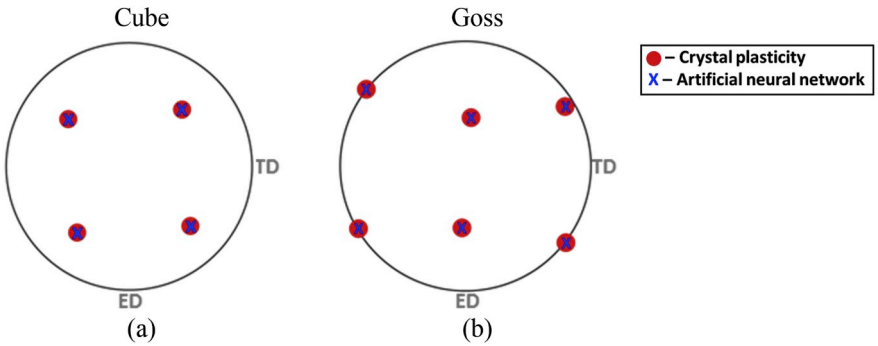

Fig. 9. Uniaxial tensile < 1 1 1 > pole figure comparison between crystal plasticity and artificial neural network (a) Cube and (b) Goss single crystals at 10% strain. Corresponding errors between crystal plasticity and artificial neural simulations are given in Table 2.

Table 2
Combined training, validation and testing mean squared errors for single crystal ANN model results.

	MSE for Stress-strain	MSE for Texture (°)
Cube Tension	$2.75\ 10^{-5}$	$3.22\ 10^{-4}$
Goss Tension	$2.65\ 10^{-5}$	$3.86\ 10^{-4}$
Cube Shear	$3.62\ e^{-5}$	$3.01\ 10^{-4}$
Goss Shear	$3.71\ 10^{-5}$	$4.72\ 10^{-4}$

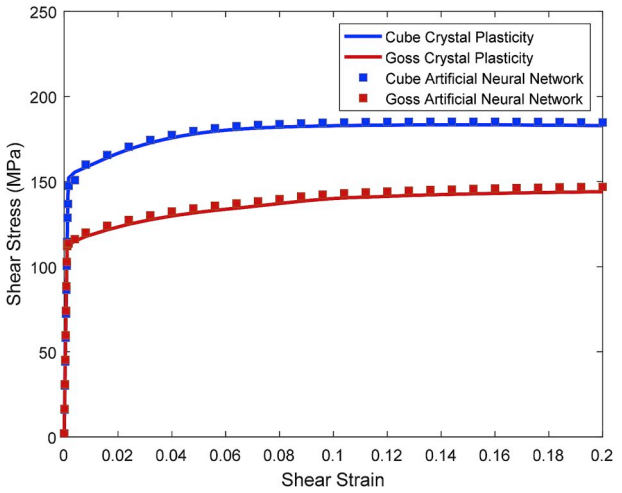

Fig. 10. Comparison between crystal plasticity and artificial neural network single crystal stress-strain curves under simple shear.

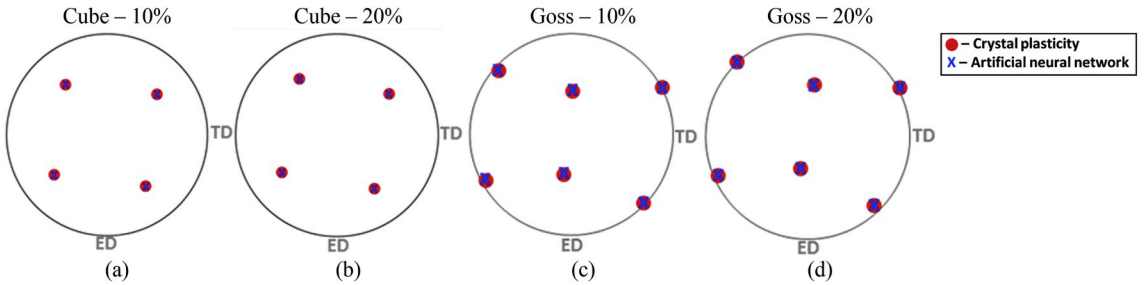

Fig. 11. Simple shear < 1 1 1 > pole figure comparison between crystal plasticity simulations and artificial neural network results at 10% and 20% strain for (a) & (b) Cube and (c) & (d) Goss single crystals respectively. Corresponding errors between crystal plasticity and artificial neural simulations are given in Table 2.

4.2.2. ANN prediction for AA6063-T6 polycrystal under tension and shear

Section 3.2.1 shows the effectiveness of the ANN model in predicting single crystal results under tension and shear with minimal errors. In this section, ANN model is applied on a real material (AA6063 – T6) under tension and shear. Results from ANN model are compared to the experimentally verified crystal plasticity results under tension and shear up to 10% and 20% strain respectively (Section 3.1). Crystal plasticity data for 3730 elements was parsed at random between the training (75%), validating (15%) and testing (15%) data sets for the ANN model using 80 neurons.

Fig. 12 shows the crystal plasticity and ANN uniaxial stress-strain response. ANN predictions show an excellent agreement with crystal plasticity results under tension for the complete stress-strain curve. Fig. 13 shows the corresponding < 1 1 1 > pole figures at 10% strain for crystal plasticity and ANN respectively. ANN results show excellent agreement with crystal plasticity results and are able to capture the trends and intensities of the evolved texture after tension with minor differences near the center of the pole figure. The corresponding MSE under tension for AA6063-T6 polycrystal stress-strain and texture response are given in Table 3 and are on the order of 10^{-4} and 10^{-2} for stress-strain and texture predictions respectively.

Crystal plasticity and ANN stress-strain response of polycrystalline AA6063-T6 under shear deformation is shown in Fig. 14. ANN model shows an excellent agreement with the crystal plasticity results. Fig. 15 shows the crystal plasticity and ANN < 1 1 1 > pole figures at 10% and 20% shear strain. Pole figures at two strain points show the rotation in texture due to shear deformation. ANN model shows good agreement with the crystal plasticity results at 10% and 20% strain and is also able to capture the pole intensities

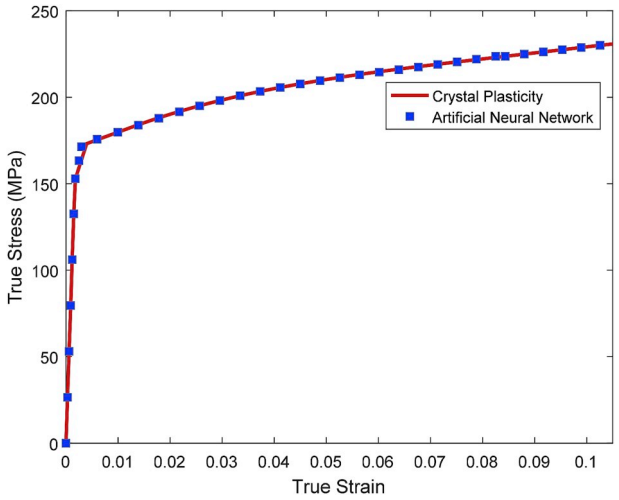

Figure 12. Comparison between crystal plasticity and artificial neural network stress-strain curves under uniaxial tension for AA 6063 – T6 polycrystal.

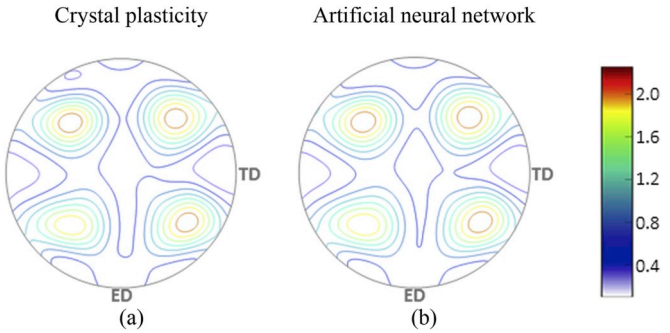

Fig. 13. Tensile < 1 1 1 > pole figure comparison between (a) Crystal plasticity simulations and (b) Artificial neural network results at 10% strain for AA6063 – T6 polycrystal.

Table 3
Training, validation and testing mean squared errors for AA6063-T6 polycrystal ANN model results.

	MSE Stress-strain	MSE Texture (°)
Tension test	$2.35\ 10^{-4}$	$2.13\ 10^{-2}$
Shear test	$3.36.63\ 10^{-4}$	$5.73\ 10^{-3}$

and texture rotation at 10% (5°) and 20% (11°) strain accurately. The corresponding MSE under shear for AA6063-T6 polycrystal stress-strain and texture response are given in Table 3 and are on the order of 10^{-4} and 10^{-3} for stress-strain and texture predictions respectively.

4.2.3. Advanced ANN predictions

Results from Section 4.2.2 demonstrate the predictive capabilities of the proposed ANN model. In this section, the ANN model was employed for predictions of the material response outside the bounds of the trained, validated and tested data. Furthermore, non-proportional loading conditions (i.e. simple shear – uniaxial tension and uniaxial tension – simple shear) were also simulated to evaluate the predictive capabilities of the proposed model. A well-defined, properly trained ANN model should, in principle, be able to provide reasonably good predictions outside the bounds of its training data set and as well as predictions of non-proportional loading cases. On the other hand, a weak model would show erroneous results (Aghasafari et al., 2014).

As simple shear deformation, by nature, presents relatively more complex stress-strain and texture evolution, the ANN model was tested for predicting the material response during simple shear between 20% and 30% strain. It is noted, that in previous sections, the ANN model was only trained, validated and tested from 0 to 20% strain and therefore had not seen any data after 20% strain. Fig. 16 shows the crystal plasticity and ANN stress-strain prediction between 20% and 30% strain whileFig. 17 presents the corresponding

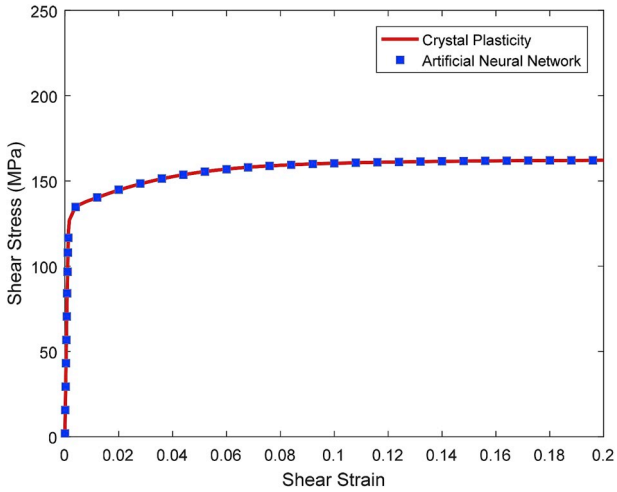

Fig. 14. Comparison between crystal plasticity and artificial neural network stress-strain curves under simple shear for AA 6063 – T6 polycrystal.

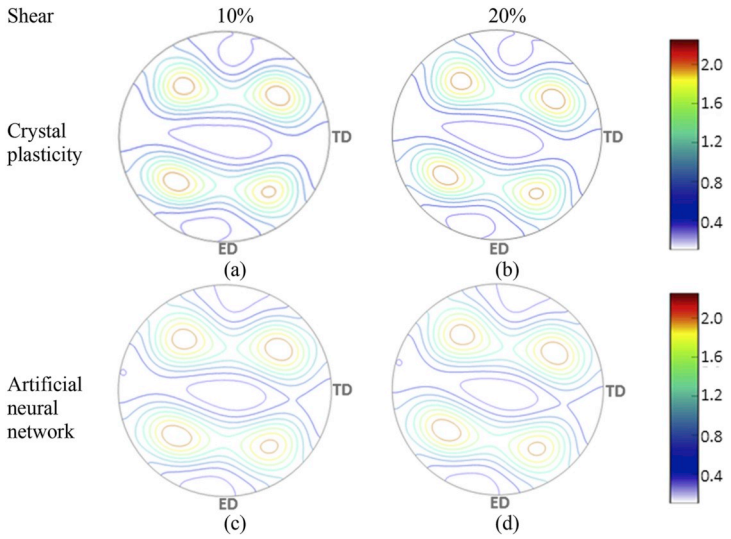

Fig. 15. Simple shear < 1 1 1 > pole figure comparison between (a) & (b) Crystal plasticity simulations at 10% and 20% strain and (c) & (d) Artificial neural network results at 10% and 20% strain for AA6063 – T6 polycrystal respectively.

pole figures from the crystal plasticity and ANN predictions at 25% and 30% strain respectively. It can be seen that the ANN model shows very good agreement, in terms of stress-strain and texture evolution, with the corresponding crystal plasticity simulations. As predictions after 20% strain were outside the bounds of the ANN model, the MSE for stress-strain ($2.43\ 10^{-3}$) and texture ($3.71\ 10^{-2}$) predictions show a slight increase in MSE than the polycrystal results from Section 4.2.2 (see Fig. 17).

Even though, the monotonic strain paths employed in previous sections provide enough confidence in the predictive capability of the proposed ANN model, it is important to validate the ANN model with non-proportional complex loading conditions (Bouvier et al., 2006; Muhammad et al., 2015). For this purpose, two separate simulations were performed and the results were compared against the corresponding crystal plasticity predictions. In the first case, the ANN model predictions of uniaxial tension up to 10% strain (along the ED) followed by simple shear up to 10% strain (along the TD) were compared to crystal plasticity simulations (tensile – shear). This was followed with the second case, where the ANN model predictions of simple shear (along TD) up to 10% strain followed by uniaxial tension up to 10% strain (along the ED) were compared to crystal plasticity simulations (shear-tension). Fig. 18a and b present the predicted tension-shear and shear-tension responses respectively. It should be noted that the tensile and shear strains are shown on the two-separate x-axis combined together for brevity while the shear stress and tensile stress are shown on separate y-axis. The analyses show that, predictions with the ANN model of both tension-shear and shear-tension present excellent agreement with crystal plasticity simulations (Fig. 18a and b). The corresponding MSE for shear-tension and tension-shear were calculated to be $4.91\ 10^{-3}$ and $9.14\ 10^{-3}$, respectively. Finally, it should be mentioned that no extra training was performed for the ANN model; the same ANN model employed in Section 4.2.2 was used to simulate tension-shear and shear-tension strain paths.

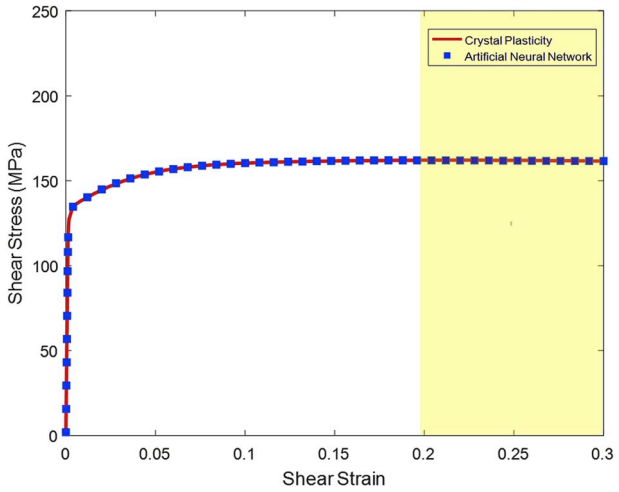

Fig. 16. Comparison between crystal plasticity and artificial neural network stress-strain curves under simple shear for AA 6063 – T6 polycrystal from 20% to 30% strain.

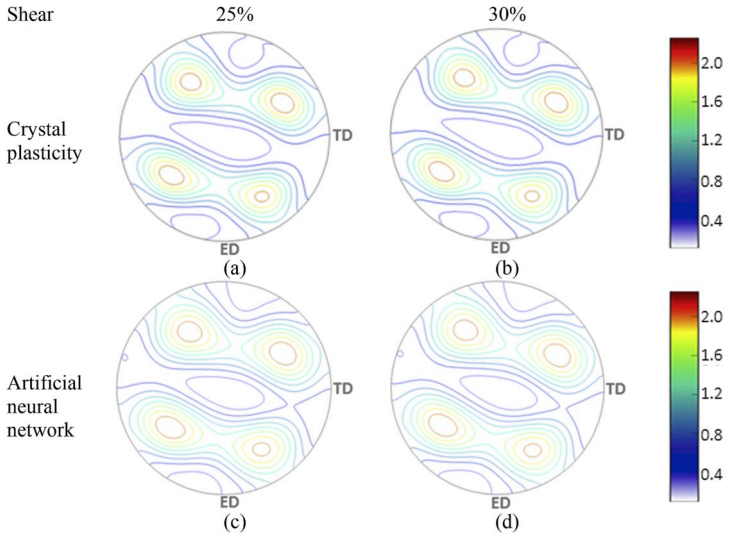

Fig. 17. Simple shear < 1 1 1 > pole figure comparison between (a) & (b) Crystal plasticity simulations at 25% and 30% strain and (c) & (d) Artificial neural network results at 25% and 30% strain for AA6063 – T6 polycrystal.

4.3. Runtime comparison

Results from previous sections show the strength of ANN model to predict the stress-strain and texture evolution behavior of single crystals and polycrystalline materials subjected to multiple strain paths. However, one of the biggest advantages of machine learning approaches, such as artificial neural network, is the huge computational improvements over conventional simulation tools. These computational savings come from the fact that once an ANN model is trained and validated, the model does not need to run computationally expensive simulations to regenerate or predict the data. Therefore, ANN models take only a fraction of the time compared to numerical simulations.

It is well known that crystal plasticity simulations, while being able to accurately predict the material response under various loading conditions (Brahme et al., 2011), require a lot of computational power for solving non-linear differential equations and many attempts have been made to speed-up crystal plasticity simulations including parallel computing (Inal, 2001). Therefore, crystal plasticity finite element simulations and the proposed ANN model were compared to analyze the computational advantage of using ANN models.

Fig. 19 shows the runtime comparison between crystal plasticity and ANN predictions from 560 to 5500 elements. As the same experimental EBSD data is used as input to the ANN model, various mesh sizes were used (16 μm–50 μm) to achieve the variation in number of elements. It is noted that the runtime comparison in seconds (*s*) is plotted in log scale to highlight the huge time difference between the two approaches. For example, to predict the stress-strain and texture response for 500 elements, ANN takes 0.04 *s*

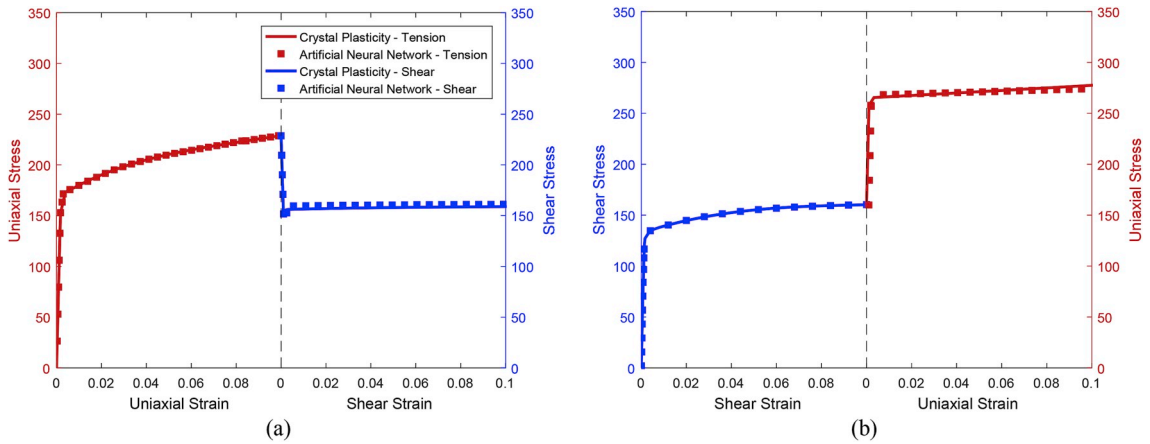

Fig. 18. Comparison between crystal plasticity and artificial neural network stress-strain curves under non-proportional loading (a) 10% uniaxial tension followed by 10% shear and (b) 10% shear followed by 10% uniaxial tension. In both figures, the red and blue color correspond to the uniaxial tension and simple shear response respectively. (For interpretation of the references to color in this figure legend, the reader is referred to the Web version of this article.)

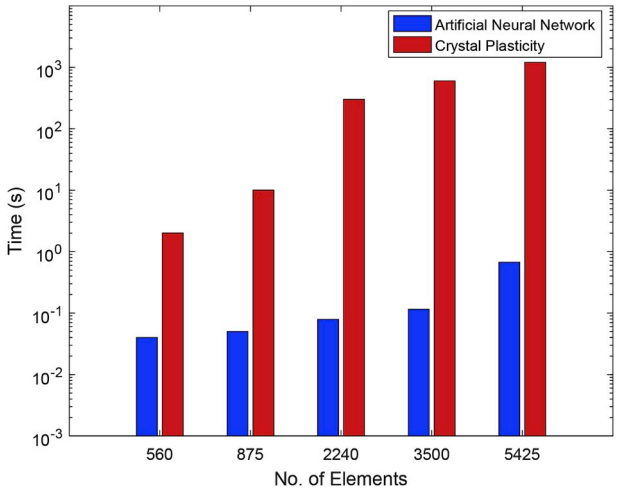

Fig. 19. Runtime comparison between crystal plasticity and the proposed artificial neural network model. Log scale is used on the vertical Y-axis to demonstrate the magnitude of orders of time difference between the two methods.

compared to crystal plasticity simulations (2 *s*). It should be mentioned that, due to the initial microstructure (morphology and texture) relatively large number of elements could be required for accurate predictions with the CPFEM approach (Brahme et al., 2012). However, as these numerical models are based on finite element methods, an exponential increase is observed in computational time as more elements are used. Results presented in Fig. 19 show that for a more than 2200 elements, the proposed model results in a computational time savings of 99.9%. It is noted that the results presented in this section highlight the usefulness of ANN models in terms of not only their predictive capability but also their computational time savings.

As is demonstrated in this work, ANN models are capable of capturing the non-linear polycrystalline material behavior and complex microstructure evolution under different loading conditions. The success of this approach motivates further use of Machine Learning techniques, such as ANN based models, as a powerful tool for alloy development, design and computationally efficient numerical simulations over conventional modelling techniques.

5. Summary and conclusions

In this paper, a coupled crystal plasticity - artificial neural network (ANN) based framework is proposed to model the stress-strain and texture evolution in single and polycrystal AA6063-T6 under tension and shear with huge computational time savings. While it is possible to increase the accuracy of CPFEM predictions with various approaches (i.e., mechanism based hardening models and/or large EBSD map as input), the main goal of this research is to demonstrate that ANN can significantly decrease the computational cost for crystal plasticity based applications. To the best knowledge of authors, this is the first work presented to predict the stress-strain

and texture evolution under tension and shear using machine learning techniques; such as ANN models.

The important conclusions are as follows:

1. Comparison of stress-strain and texture evolution data from CPFEM formulation shows good agreement with experimental measurements. This experimentally validated data is used as input to train, validate and test the proposed ANN model.
2. Proposed ANN model shows very good predictions for stress-strain and texture evolution for AA6063-T6 polycrystal results under tension and shear. In addition, ANN model is able to capture the pole figure trends and intensities with minimal error.
3. The proposed ANN model presents excellent predictive capabilities for stress-strain and texture evolution responses outside the bounds of the original data set. In addition, the predictive capability of the proposed ANN model is further demonstrated by successfully predicting the material responses subjected to non-proportional loading paths such as uniaxial tension followed by simple shear and simple shear followed by uniaxial tension.
4. As was the main objective of this work, the proposed ANN model shows upto 99.9% computational speedup over conventional crystal plasticity finite element methods based numerical models.

Acknowledgements

This work was supported by the Natural Sciences and Engineering Research Council of Canada under grant no. APCPJ 441668-12. The authors would also like to acknowledge the high-performance computing center at the University of Sherbrooke and would like to acknowledge help from Professor William Melek at University of Waterloo.

References

Aghasafari, P., Abdi, H., Salimi, M., 2014. Artificial neural network modeling of flow stress in hot rolling. ISIJ Int. 54 (4), 872–879.
Akpama, H.K., Ben Bettaieb, M., Abed-Meraim, F., 2016. Numerical integration of rate-independent BCC single crystal plasticity models: comparative study of two classes of numerical algorithms. Int. J. Numer. Methods Eng. 108 (5), 363–422.
Ali, U., Odoh, D., Muhammad, W., Brahme, A., Mishra, R.K.R.K., Wells, M., Inal, K., Jul. 2017. Experimental investigation and through process crystal plasticity-static recrystallization modeling of temperature and strain rate effects during hot compression of AA6063. Mater. Sci. Eng. A 700, 374–386.
Asaro, R.J., Needleman, A., 1985. Texture development and strain hardening in rate dependent polyrystals. Acta Metall. 33 (42), 923–953.
Bhadeshia, H.K.D.H., 1999. Neural networks in materials science. ISIJ Int. 39 (10), 966–979.
Bishop, C.M., 2006. Pattern Recognition and Machine Learning. Springer.
Bouvier, S., Gardey, B., Haddadi, H., Teodosiu, C., 2006. Characterization of the strain-induced plastic anisotropy of rolled sheets by using sequences of simple shear and uniaxial tensile tests. J. Mater. Process. Technol. 174 (1), 115–126.
Brahme, A., Winning, M., Raabe, D., 2009. Prediction of cold rolling texture of steels using an Artificial Neural Network. Comput. Mater. Sci. 46 (4), 800–804.
Brahme, A.P., Inal, K., Mishra, R.K., Saimoto, S., Aug. 2011. A new strain hardening model for rate-dependent crystal plasticity. Comput. Mater. Sci. 50 (10), 2898–2908.
Brahme, A., Staraselski, Y., Inal, K., Mishra, R.K., 2012. Determination of the minimum scan size to obtain representative textures by electron backscatter diffraction. Metall. Mater. Trans. A Phys. Metall. Mater. Sci. 43 (13), 5298–5307.
Çetinel, H., Özyiğit, H.A., Özsoyeller, L., Feb. 2002. Artificial neural networks modeling of mechanical property and microstructure evolution in the Tempcore process. Comput. Struct. 80 (3–4), 213–218.
Chang, Y.W., Asaro, R.J., 1981. An experimental study of shear localization in aluminum-copper single crystals. Acta Mater. 29, 241–257.
Cherkassky, V., Lari-Najafi, H., 1990. Self-organizing neural network for non-parametric regression analysis. In: International Neural Network Conference, pp. 838.
Diard, O., Leclercq, S., Rousselier, G., Cailletaud, G., 2005. Evaluation of finite element based analysis of 3D multicrystalline aggregates plasticity. Int. J. Plast. 21 (4), 691–722.
Ghaboussi, J., Garrett, J.H., Wu, X., 1991. "Knowledge-Based modeling of material behavior with neural networks. J. Eng. Mech. 117 (1), 132–153.
Ghaffari Tari, D., Worswick, M.J.J., Ali, U., Gharghouri, M.A.A., 2014. Mechanical response of AZ31B magnesium alloy: experimental characterization and material modeling considering proportional loading at room temperature. Int. J. Plast. 55, 247–267.
Guessasma, S., Coddet, C., Oct. 2004. "Microstructure of APS alumina–titania coatings analysed using artificial neural network. Acta Mater. 52 (17), 5157–5164.
Haghdadi, N., Zarei-Hanzaki, A., Khalesian, A.R., Abedi, H.R., Aug. 2013. Artificial neural network modeling to predict the hot deformation behavior of an A356 aluminum alloy. Mater. Des. 49, 386–391.
Hansen, K., Montavon, G., Biegler, F., Fazli, S., Rupp, M., Scheffler, M., Von Lilienfeld, O.A., Tkatchenko, A., Miller, K.R., 2013. Assessment and validation of machine learning methods for predicting molecular atomization energies. J. Chem. Theory Comput. 9 (8), 3404–3419.
Inal, K., 2001. Numerical Simulation of Sheet Metal Forming Processes and Localized Deformation Phenomena for FCC Polycrystals. PhD Thesis. Université de Sherbrooke, Sherbrooke, QC.
Inal, K., Wu, P.D., Neale, K.W., Jun. 2002. Finite element analysis of localization in FCC polycrystalline sheets under plane stress tension. Int. J. Solids Struct. 39 (13–14), 3469–3486.
Jenab, A., Karimi Taheri, A., Jenab, K., 2013. The use of ANN to predict the hot deformation behavior of AA7075 at low strain rates. J. Mater. Eng. Perform. 22 (3), 903–910.
LeCun, Y.A., Bottou, L., Orr, G.B., Müller, K.-R., 2012. Efficient BackProp. In: Montavon, G., Orr, G.B., Müller, K.-R. (Eds.), Neural Networks: Tricks Of the Trade, second ed. Springer Berlin Heidelberg, Berlin, Heidelberg, pp. 9–48.
Lin, Y.C., Zhang, J., Zhong, J., Oct. 2008a. Application of neural networks to predict the elevated temperature flow behavior of a low alloy steel. Comput. Mater. Sci. 43 (4), 752–758.
Lin, Y.C., Fang, X., Wang, Y.P., 2008b. Prediction of metadynamic softening in a multi-pass hot deformed low alloy steel using artificial neural network. J. Mater. Sci. 43 (16), 5508–5515.
Liu, R., Kumar, A., Chen, Z., Agrawal, A., Sundararaghavan, V., Choudhary, A., 2015. A predictive machine learning approach for microstructure optimization and materials design. Sci. Rep. 5 (1), 11551.
Montavon, G., Müller, K.-R., 2012. Deep Boltzmann machines and the centering trick. In: Neural Networks: Tricks of the Trade. Springer, pp. 621–637.
Muhammad, W., Mohammadi, M., Kang, J., Mishra, R.K., Inal, K., 2015. An elasto-plastic constitutive model for evolving asymmetric/anisotropic hardening behavior of AZ31B and ZEK100 magnesium alloy sheets considering monotonic and reverse loading paths. Int. J. Plast. 70, 30–59.
Muhammad, W., Brahme, A., Kang, J., Mishra, R.K., Inal, K., 2017. Experimental and numerical investigation of texture evolution and the effects of intragranular backstresses in aluminum alloys subjected to large strain cyclic deformation. Int. J. Plast. 137, 137–163.
Nielsen, M., 2015. Neural Networks and Deep Learning. *Determ. Press*.
Pandey, A., Khan, A.S., Kim, E.-Y., Choi, S.-H., Gnäupel-Herold, T., 2012. Experimental and numerical investigations of yield surface, texture, and deformation

mechanisms in AA5754 over low to high temperatures and strain rates. Int. J. Plast. 41, 165–188.
Plunkett, B., Cazacu, O., Barlat, F., 2008. Orthotropic yield criteria for description of the anisotropy in tension and compression of sheet metals. Int. J. Plast. 24 (5), 847–866.
Popova, E., Staraselski, Y., Brahme, A., Mishra, R.K., Inal, K., 2015. Coupled crystal plasticity - probabilistic cellular automata approach to model dynamic re-crystallization in magnesium alloys. Int. J. Plast. 66, 85–102.
Qin, Y.J., Pan, Q.L., He, Y.B., Li, W.B., Liu, X.Y., Fan, X., 2010. Artificial neural network modeling to evaluate and predict the deformation behavior of ZK60 magnesium alloy during hot compression. Mater. Manuf. Process. 25 (7), 539–545.
Raabe, D., 2002. Challenges in computational materials science. Adv. Mater. 14 (9), 639–650.
Reddy, N.S., Rao, A.K.P., Chakraborty, M., Murty, B.S., Jan. 2005. "Prediction of grain size of Al–7Si Alloy by neural networks. Mater. Sci. Eng. A 391 (1–2), 131–140.
Rossiter, J., Brahme, A., Simha, M.H.H., Inal, K., Mishra, R.K., Dec. 2010. A new crystal plasticity scheme for explicit time integration codes to simulate deformation in 3D microstructures: effects of strain path, strain rate and thermal softening on localized deformation in the aluminum alloy 5754 during simple shear. Int. J. Plast. 26 (12), 1702–1725.
Rumelhart, D.E., Hinton, G.E., Williams, R.J., 1988. And others, "Learning representations by back-propagating errors. Cogn. Model. 5 (3), 1.
Sabokpa, O., Zarei-Hanzaki, A., Abedi, H.R., Haghdadi, N., 2012. Artificial neural network modeling to predict the high temperature flow behavior of an AZ81 magnesium alloy. Mater. Des. 39, 390–396.
Specht, D.F., 1991. "A general regression neural network," *Neural Networks*. IEEE Trans. 2 (6), 568–576.
Yassar, R.S., AbuOmar, O., Hansen, E., Horstemeyer, M.F., Sep. 2010. On dislocation-based artificial neural network modeling of flow stress. Mater. Des. 31 (8), 3683–3689.